

PAPER • OPEN ACCESS

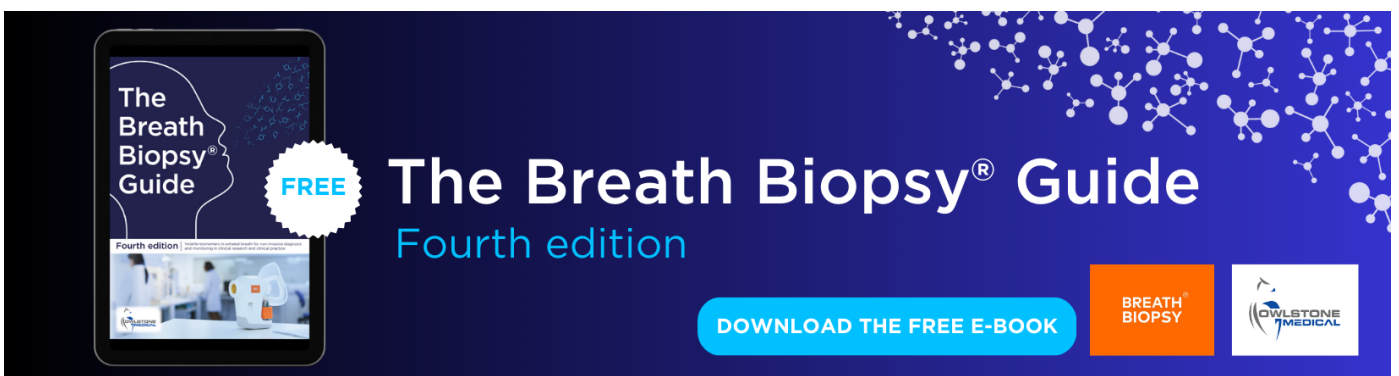
Organic-inorganic biohybrid films from wool-keratin/jellyfish-collagen/silica/boron via sol-gel reactions for soft tissue engineering applications

To cite this article: Safiye Nur Yildiz *et al* 2024 *Biomed. Mater.* **19** 025032

View the [article online](#) for updates and enhancements.

You may also like

- [d/dy distribution of Drell-Yan dielectron pairs at CDF](#)
J Han, A Bodek, W Sakumoto et al.
- [Time Delay of Mg ii Emission Response for the Luminous Quasar HE 0435-4312: toward Application of the High-accretor Radius-Luminosity Relation in Cosmology](#)
Michal Zajaek, Boena Czerny, Mary Loli Martinez-Aldama et al.
- [Irradiation hardening behaviors of tungsten-potassium alloy studied by accelerated 3-MeVW²⁺ ions](#)
Xiao-Liang Yang, , Long-Qing Chen et al.



The Breath Biopsy® Guide
Fourth edition

FREE

DOWNLOAD THE FREE E-BOOK

BREATH BIOPSY

OWLSTONE MEDICAL

Biomedical Materials



PAPER

OPEN ACCESS

RECEIVED
22 November 2023

REVISED
15 January 2024

ACCEPTED FOR PUBLICATION
2 February 2024

PUBLISHED
13 February 2024

Original content from this work may be used under the terms of the [Creative Commons Attribution 4.0 licence](https://creativecommons.org/licenses/by/4.0/).

Any further distribution of this work must maintain attribution to the author(s) and the title of the work, journal citation and DOI.



Organic-inorganic biohybrid films from wool-keratin/jellyfish-collagen/silica/boron via sol-gel reactions for soft tissue engineering applications

Safiye Nur Yildiz , Tugba Sezgin Arslan and Yavuz Emre Arslan*

Regenerative Biomaterials Laboratory, Department of Bioengineering, Faculty of Engineering, Canakkale Onsekiz Mart University, Canakkale 17100, Turkey

* Author to whom any correspondence should be addressed.

E-mail: yavuzzea@gmail.com

Keywords: jellyfish collagen, wool keratin, boron, organic-inorganic biohybrid, sol-gel, regenerative medicine, CAM assay

Supplementary material for this article is available [online](#)

Abstract

Therapeutic angiogenesis is pivotal in creating effective tissue-engineered constructs that deliver nutrients and oxygen to surrounding cells. Hence, biomaterials that promote angiogenesis can enhance the efficacy of various medical treatments, encompassing tissue engineering, wound healing, and drug delivery systems. Considering these, we propose a rapid method for producing composite silicon-boron-wool keratin/jellyfish collagen (Si-B-WK/JFC) inorganic-organic biohybrid films using sol-gel reactions. In this approach, reactive tetraethyl orthosilicate and boric acid ($pK_a \geq 9.24$) were used as silicon and boron sources, respectively, and a solid-state gel was formed through the condensation reaction of these reactive groups with the keratin/collagen mixture. Once the resulting gel was thoroughly suspended in water, the films were prepared by a casting/solvent evaporation methodology. The fabricated hybrid films were characterized structurally and mechanically. In addition, angiogenic characteristics were determined by the in ovo chick chorioallantoic membrane assay, which revealed an increased vascular network within the Si-B-WK/JFC biohybrid films. In conclusion, it is believed that Si-B-WK/JFC biohybrid films with mechanical and pro-angiogenic properties have the potential to be possessed in soft tissue engineering applications, especially wound healing.

1. Introduction

With the globally increasing healthy life expectancy and human longevity, developing new materials to treat age-related diseases and repair lost or damaged tissues and organs has become necessary [1]. Developed biomaterials must have mechanical (stiffness, elastic modulus, etc) physicochemical (surface chemistry, porosity, biodegradation, etc) and biological properties (cell adhesion, vascularization, biocompatibility, etc) to reconstruct different anatomical defects of complex organs and functional tissues [2].

In material science and engineering, several methods and procedures have been used to construct many biomaterials in different fields, such as drug delivery, wound healing, and tissue engineering applications.

Based on their chemical composition, biomaterials can be divided into five categories: metals, bio-ceramics, natural and synthetic polymers, and composites [3]. Unlike synthetic polymers, natural bio-based materials are preferred for bioscaffold production due to their appealing properties, such as biological activity, biodegradation rate, natural abundance, mimicking of the extracellular matrix (ECM), and low cost [4, 5]. Natural polymers can be obtained from different biological sources, such as plants, animals, and microorganisms, and have been recognized as an attractive choice for tissue engineering applications. Renewable materials, such as keratin, collagen, elastin, silk fibroin, etc, obtained from animal/insect wastes, have been utilized in biomedicine and biotechnology in various forms, including scaffolds, coatings, hydrogels, and films. Keratin,

obtained from keratinous waste materials, is a fibrillar protein that forms the epidermis structure and its appendages, including hair, wool, feathers, nails, horns, and hooves. Collagen, the main protein of connective tissue, is abundant in the tendon, bone, and cartilage tissues and is mainly isolated from these sources [6]. However, due to the risk of spreading bovine spongiform encephalopathy and prion diseases, marine sources such as commercial fish, sharks, and jellyfish have recently been used instead of mammalian collagen [7].

There is a substantial demand for the development of innovative scaffolds to keep up with the latest technological advancements. Given that situation, it can be said that organic-inorganic nanocomposites that combine the properties of both materials in a single hybrid structure offer an intriguing strategy to enhance the characteristics of good mechanical strength and thermal and chemical stability. More importantly, they can significantly impact permeability and selectivity due to the controllable pore size and distribution in their structures [8].

Sol-gel reaction as a wet chemistry-driven synthesis method is a well-known technique that can be used to produce functional and innovative hybrid materials, including glass, ceramics, and organic/inorganic hybrids. In this technique, once a precursor solution such as tetraethyl orthosilicate (TEOS) is hydrolyzed in an acidic or basic medium, siloxane structures are formed due to condensation and polycondensation reactions between the resulting reactive silanol groups. The sol-gel process offers considerable advantages, such as easy incorporation of organic-inorganic frameworks into the polymeric network, solid and porous network gel formation, and mild reaction conditions [9, 10].

One of our previous works reported that inorganic materials such as silicon and boron are trace elements in the human body and contribute to wound healing and bone homeostasis by binding to ECM components such as collagen, glycosaminoglycans, and proteoglycans [11, 12]. Moreover, Kakkar and Madhan also stated that the hybrid biomaterials containing silicon induce the proliferation of fibroblasts and osteoblasts that support collagen formation. They fabricated sol-gel based keratin/silica hybrid material with high mechanical properties for the wound healing process [13]. Silicon-boron containing glycerohydrogel [14], mupirocin silica microspheres loaded collagen [15], and chitosan-silica dressing incorporated with keratinocyte growth factor [16] are the other substantial hybrid wound dressing materials fabricated via sol-gel method.

The current study is directed at synthesizing sol-gel based novel organic-inorganic hybrid films. In this regard, three kinds of hybrid films were synthesized, namely silicon-boron-wool keratin (Si-B-WK),

silicon-boron-jellyfish collagen (Si-B-JFC), and silicon-boron-wool keratin/jellyfish collagen (Si-B-WK/JFC). A comprehensive analysis assessed the hybrid films' structural, physico/biochemical, and mechanical characteristics. In ovo chick chorioallantoic membrane (CAM) assay was also conducted to test the biocompatibility and vasculogenic potential of the biohybrid films.

2. Experimental section

2.1. Materials

Wool samples were provided from a local farm in Çanakkale, Türkiye. *Rhizostoma pulmo*, commonly known as the barrel jellyfish, was caught in the Dardanelles (Abydus), Çanakkale, Türkiye. Sodium hydroxide (NaOH, 98%–100.5%, pellets), sodium sulfite (Na₂SO₃, anhydrous), TEOS (reagent grade, 98%, TEOS), hydrochloric acid (HCl), boric acid (H₃BO₃, ≥99.5%), acetic acid (99.8%–100.5%), pepsin (powder, slightly beige, 500 U mg⁻¹), 2-(N-morpholino) ethane sulfonic acid (MES, ≥99%), N-hydroxysuccinimide (NHS, 98%), N-(3-dimethylamino propyl)-N'-ethyl carbodiimide hydrochloride (EDC, 8.00907.0025), ethyl alcohol (≥99.5%, EtOH), proteinase K from *Tritirachium* (lyophilized powder, ≥30 units mg⁻¹ protein), were purchased from Merck (Germany).

2.2. Preparation of pepsin soluble jellyfish collagen (PS-JFC) and wool keratin (WK)

Collagen derived from jellyfish was extracted according to our previous studies with a moderate modification [17, 18]. Keratin was also extracted from wool using a sulphitolysis reaction previously reported by our group [12]. The extraction steps of PS-JFC and WK are given in figures 1(A) and (B), respectively, and the relevant protocols are outlined in the supporting information file (SI-1 and SI-2).

2.3. Biochemical analyses of PS-JFC and WK extracts

WK and PS-JFC were extracted in our previous studies, and biochemical characterization, such as sodium dodecyl sulfate-polyacrylamide gel electrophoresis (SDS-PAGE), amino acid content analysis, etc, was carried out in detail. Since protein extracts obtained through the same method were used in our current study, the mentioned analyses were not replicated. However, a Lowry protein assay was conducted to determine the protein content of WK and PS-JFC extracts. Ellman's assay was also performed to determine free sulfhydryl groups in WK extracts using Ellman's reagent. The analyses above and the required equations were detailed in our previous studies [12, 17, 18].

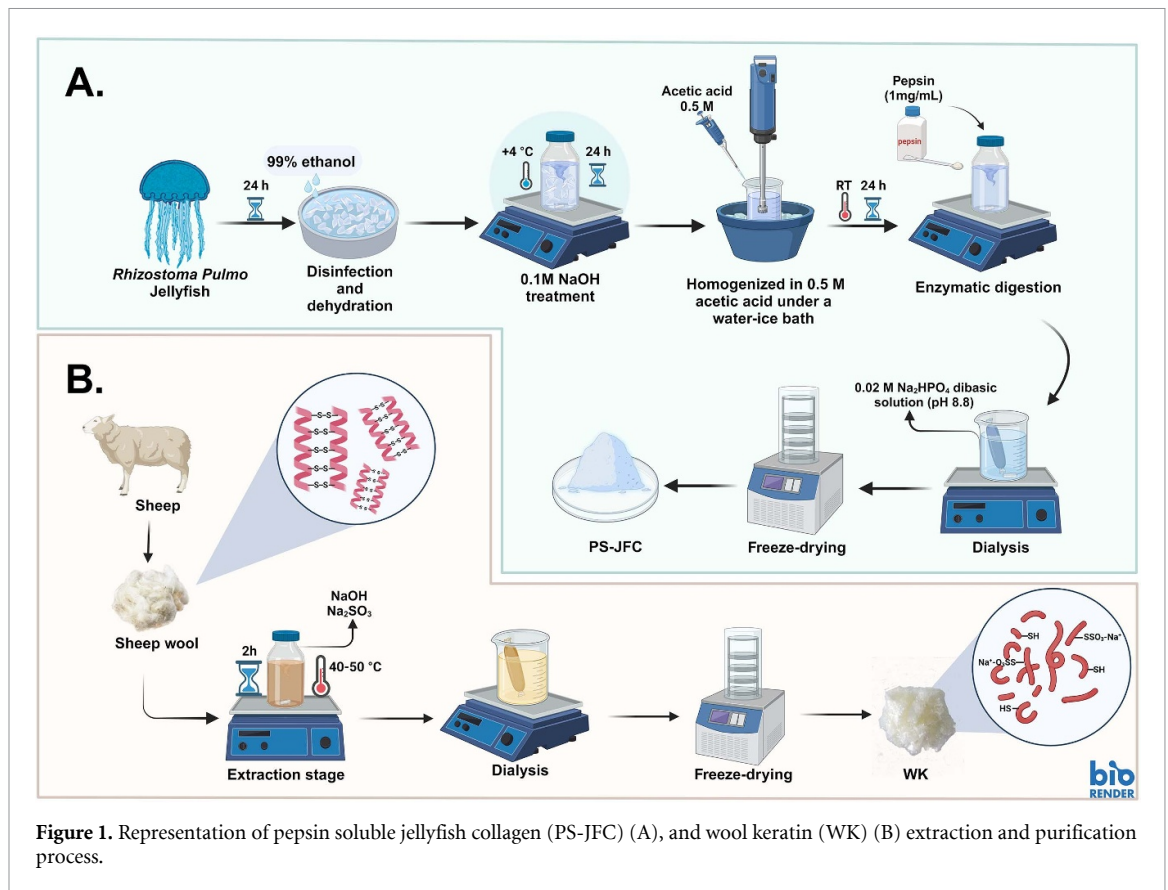


Figure 1. Representation of pepsin soluble jellyfish collagen (PS-JFC) (A), and wool keratin (WK) (B) extraction and purification process.

2.4. Synthesis of organic-inorganic biohybrid films

First, the reactive TEOS (rTEOS) was obtained by slightly modifying the reaction conditions according to the study of Yuan and No [19]. Briefly, a mixture consisting of TEOS (1.1 ml), HCl (0.1 M, 0.125 ml), and Milli-Q water (0.816 ml) (Milli Direct-Q 3UV, 18 MΩ cm⁻¹ at 25 °C, Merck-Millipore, Germany) was vigorously stirred for 5 min in a glass vial at room temperature. Subsequently, the mixture was exposed to ultrasonic agitation at 45 °C for 10 min until a clear solution was achieved. The prepared stock solution was made daily, used freshly, and then stored at ambient temperature (figure 2(A)). Boric acid was dissolved in water at a concentration of 3% (w/v), and then the solution pH was adjusted to ≥ 9.24 (equal or greater than the pKa of boric acid) by dropwise addition of 1 M NaOH to obtain reactive tetrahydro borate anions (figure 2(B)). PS-JFC was first dissolved at a concentration of 5% (w/v) in boric acid (pH ≥ 9.24) by using an ultrasonic bath. An equal amount of WK (5% w/v) was added to this solution, mixing gently without foaming. To reduce brittleness and increase film flexibility, glycerol, a plasticizing polyol, was added to the protein solution at a concentration of 10% (v/v). To initiate the sol-gel reaction, rTEOS and protein solution were mixed thoroughly at 1:10 (v/v), respectively. The resulting mixture was left to rest at room temperature overnight to complete the sol-gel

transformation and mature the gel. The solid gel was then mixed with pure water at a ratio of 1:4 and exposed to ultrasound agitation until well-dispersion was achieved. A volume of 5 ml from this mixture was poured into round-shaped silicone molds. After the solvent was evaporated by an incubator set at constant temperature (40 °C) and relative humidity (RH) (60%), The produced soft films were cured at 110 °C for 2 h to extract films easily from the mold by eliminating excess glycerol (figure 2(C)). Finally, a transparent, translucent, and brownish organic-inorganic Si-B-WK/JFC hybrid film was achieved. Similar reactions were repeated for sol-gel reactions and film production after preparing 10% (w/v) of keratin and 5% (w/v) of collagen solutions in boric acid. Thus, Si-B-WK and Si-B-JFC inorganic-organic films were obtained as well. (figures 2(D) and (E)). The network structure of the formed inorganic-organic biohybrid films is given in figure 2(F). To improve mechanical properties, all inorganic-organic hybrid films were cross-linked for 2 h at room temperature by the EDC/NHS method, as described in our previous study [12]. The mechanism of the coupling reactions between keratin and collagen in the Si-B-WK/JFC organic-inorganic biohybrid network is also presented in figure 2(G). The coupling mechanism of NHS/EDC is also detailed in the supporting information file (SI-3, figure S1). The resulting films were

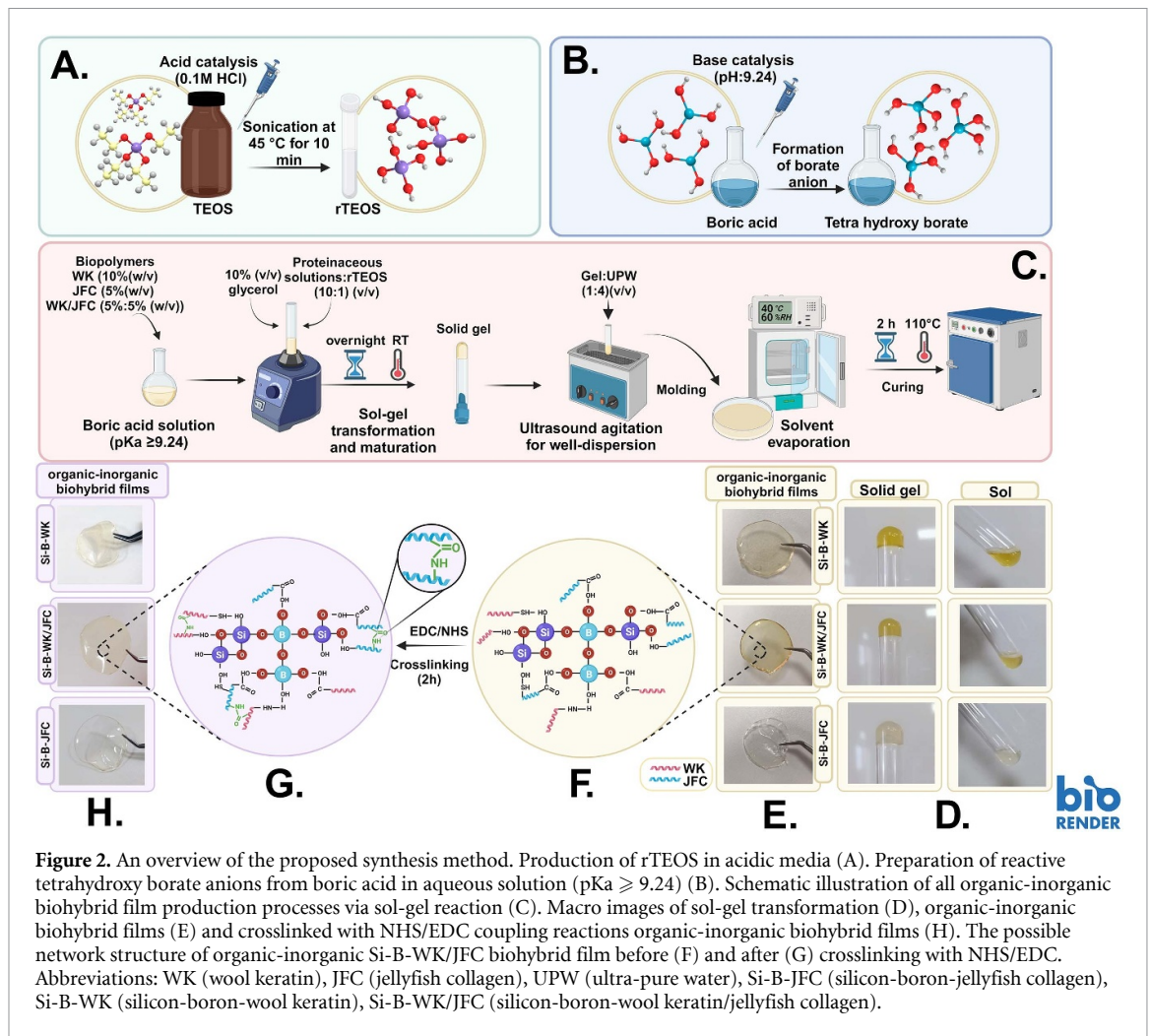


Figure 2. An overview of the proposed synthesis method. Production of rTEOS in acidic media (A). Preparation of reactive tetrahydroxy borate anions from boric acid in aqueous solution ($pK_a \geq 9.24$) (B). Schematic illustration of all organic-inorganic biohybrid film production processes via sol-gel reaction (C). Macro images of sol-gel transformation (D), organic-inorganic biohybrid films (E) and crosslinked with NHS/EDC coupling reactions organic-inorganic biohybrid films (H). The possible network structure of organic-inorganic Si-B-WK/JFC biohybrid film before (F) and after (G) crosslinking with NHS/EDC. Abbreviations: WK (wool keratin), JFC (jellyfish collagen), UPW (ultra-pure water), Si-B-JFC (silicon-boron-jellyfish collagen), Si-B-WK (silicon-boron-wool keratin), Si-B-WK/JFC (silicon-boron-wool keratin/jellyfish collagen).

washed with Milli-Q water under ambient conditions to remove any residue or excessive reagents. More durable and flexible biohybrid films (figure 2(H)) were stored in a humid environment as they could be more fragile, particularly at lower relative humidities.

2.5. Physicochemical examinations of organic-inorganic biohybrid films

For the investigation of the chemical structures in the resulting hybrid films, attenuated total reflectance Fourier transform infrared spectroscopy (ATR-FTIR), solid state ^{29}Si Cross-Polarization Magic Angle Spinning (CP-MAS), and ^{11}B MAS nuclear magnetic resonance (NMR) spectroscopy and x-ray diffraction (XRD) analysis were carried out. Brunauer–Emmett–Teller (BET) and Barrett–Joyner–Halenda (BJH) methods were conducted to determine the total surface area of solid biohybrid materials. The thermal behavior of the samples was also investigated using a thermogravimetric analyzer (TGA 8000, Perkin Elmer, USA). Surface morphology and elemental mapping of hybrid films were investigated using scanning electron microscopy (SEM) and

energy dispersive x-ray analysis (FE-SEM JFM 7100F EDS) JEOL, Japan). Related analysis methods can be found in the supporting information file (SI-4). Mechanical properties such as Young's modulus, strain at break, and ultimate strength were determined by applying a uniaxial tensile test of biohybrid films on a micromechanical testing device (UniVert, CellScale Biomaterials Testing) with a 50 N load cell. A biohybrid film with a rectangular shape in a wet form (width: 12 mm, length: 14 mm, thickness: 0.2 mm) was placed between the two jaws of the device, and the tensile stiffness of the sample was determined by applying a strain rate of 0.16 mm s^{-1} until breaking occurred. Real-time images were captured using a tripod camera (HD 1080p, Logitech) at a frequency of 5 Hz throughout the measurement process. At the end of the measurement, the stress-strain curve, an essential graphical measure of a material's mechanical properties, was obtained by processing the force and displacement data. The calculation regarding Young's modulus values can be found in the supporting information file (SI-5, figure S2).

2.6. *In vitro* enzymatic biodegradation study

Striking a balance between resorption of the scaffolds and remodeling is crucial for tissue engineering applications. To track the resorption rate and the *in vitro* behaviors of the composite films, a degradation assay was conducted using protease treatment as previously described by our group [12]. Briefly, initial dry biohybrid films were weighed (m_i) and soaked in Tris-HCl buffer (0.02 M, pH 8.0) containing preservatives (sodium azide 0.05%, w/v) and proteinase K (0.01%, w/v). Samples were incubated in the enzyme solution at 37 °C for 3 and 6 d. At the end of each time point, the samples were removed, washed, lyophilized, and reweighed (m_f). The resorption rate was calculated using the equation given below:

$$\text{Weight Loss (\%)} = [(m_i) - (m_f)] / (m_i) \times 100.$$

2.7. *In ovo* CAM assay and characterizations

Chicken *in ovo* CAM assay was conducted to examine the effects of inorganic-organic hybrid films on angiogenesis and biological activity. To this end, as applied in our previous studies [20, 21], freshly fertilized chicken eggs purchased from a local provider (Çanakkale, Türkiye) were cleaned, disinfected with ethanol, and placed vertically in the rotating tray inside an egg incubator (Brinsea Ovation 28 Advance Ex, U.K.). Eggs were then incubated at 37.5 °C and 60% RH while rotating every 120 min. On the third day of embryonic development (EDD3), an opening was created at the top of the egg. Sterile parafilm was placed over the newly opened window to prevent contamination or desiccation of the egg contents. The eggs were then incubated in the egg tray in a stagnant position until material implantation. The embryos' survival rates were checked daily. On EDD7, sterile samples were placed between the prominent veins on the CAM surface using a stereomicroscope (Stemi 305, Zeiss) with a digital camera (Axiocam 105 color, Zeiss). Macroscopic images of the grafted embryos were captured on EDD7 and EDD10. The images were analyzed using ImageJ 1.51j8 (National Institutes of Health, Bethesda, MD, USA) to measure the vascular density of a 1 mm imaginary boundary drawn around the material on the CAM surface. Angiogenic response was evaluated using the vascular index, which is obtained from the ratio of vascular density at EDD10 to EDD7. The experiment was terminated after all imaging processes were completed at EDD10. The materials were excised with the CAM by leaving a 1 cm space around them. The resulting CAM-material complexes were used for SEM and histological analyses (sectioning and routine hematoxylin and eosin staining). For this purpose, all necessary processing steps were carried out as described in our previous study [21]. Until the 15th day of their development, it is generally accepted that

chick embryos do not suffer pain. Moreover, in many countries, they are not recognized as living animals before the 17th day of their embryonic development [22, 23]. Therefore, ethics approval is not required because all experiments were accomplished within 10 d.

2.8. Statistical analysis

Quantitative assays were performed in triplicate for all experiments. The data were presented in Microsoft 365 Excel as the mean \pm along with the standard deviation of the variables. Variations between the groups were assessed using OriginPro® 2023b (Origin Lab Corporation, MA, USA) software, employing a one-way analysis of variance followed by Tukey's test. When p -values were ≤ 0.05 , the difference between groups was considered significant statistically.

3. Results and discussion

3.1. Biochemical evaluations

In our previous study [12], human hair keratin was extracted by sulphitolysis reaction, and the biochemical characterization of the resulting low molecular weight (Mw) keratin extracts was investigated in depth. In this study, sheep WK, which has structurally similar properties to hair keratin [24], was extracted with the same method. According to Lowry protein analysis, the WK content in the dialysate was 8.81 ± 0.10 mg ml⁻¹, and the yield based on dry weight was about 40%. As known, during the sulphitolysis reaction, the disulfide bonds in the keratin structure are cleaved, and bunte salt (cysteine-S-sulfonate anions) and cysteine-thiol (cysteine-SH) are formed [25, 26]. A small number of reactive-SH groups can contribute to gelation by forming hydrogen bonds during the sol-gel reaction [27]. These groups were determined by the reactions with Ellman's reagent, and the amount was found to be 0.067 ± 0.009 mmol SH mg⁻¹ keratin. Findings regarding the content of keratin and free-SH groups are similar to our previous study [12]. Additionally, we performed SDS-PAGE and matrix-assisted laser desorption/ionization-time of flight (MALDI-TOF, Bruker Daltonics, Microflex LT, USA) analysis to determine the Mw distribution of keratin hydrolysates more accurately. As a result of our findings, we stated that keratin was obtained into small fractions of 2–3 kDa in size because of the highly alkaline environment used during the sulfitolysis reaction. However, many different-sized keratin fragments provide more active groups to trigger sol-gel reactions. In addition, the sulphitolysis method has the potential to be used in tissue engineering and cosmetic applications, as it is cheap, non-toxic, and has a short reaction time [12].

On the other hand, PS-JF content in the dialysate was 16 mg ml^{-1} , and the dry extract yield was also determined to be 93.5%, which shows a higher collagen recovery yield than our previous studies [17, 18]. The proposed modified method is ideal for PS-JF extraction with higher efficiency in a shorter time. Additionally, SDS-PAGE, hydroxyproline, and amino acid content analysis for the PS-JFC were performed and well-discussed in the mentioned studies.

3.2. Synthesis of organic-inorganic biohybrid films and physico-chemical evaluations

During the inorganic-organic hybrid film synthesis carried out via sol-gel reactions, the concentrations of solutions containing SW, PS-JFC, and WK/PS-JFC mixtures were adjusted at a concentration of 10% (w/v). However, Si-B-JFC biohybrid films containing 10% (w/v) of collagen and 10% (v/v) glycerol exhibited fractured surface morphology during solvent evaporation and curing processes. Therefore, the optimum amount of collagen for relatively smooth and stable film synthesis was investigated and determined as 5% (w/v). Physiochemical characterizations were performed after completing the production and optimization processes of biohybrid films.

FT-IR, NMR and XRD analyses were performed for the structural characterization of all samples. The FT-IR spectra of the WK and PS-JFC extracts and organic-inorganic biohybrid films are shown in figure 3(A). The peak of Amide A associated with the stretching vibration of N–H bonds was found between $3200\text{--}3400 \text{ cm}^{-1}$. Prominent characteristic bands helpful in explaining the conformational structures of proteins and polypeptides are amide I, amide II, and amide III bands seen in the infrared spectra. Bands that fall in the $1600\text{--}1700 \text{ cm}^{-1}$ range relate to the Amide I, demonstrating the stretching vibration of the C=O bonds. Amide II band in the $1500\text{--}1600 \text{ cm}^{-1}$ range arises primarily from N–H bending and C–H stretching vibrations. The Amide III band, susceptible to the helical structure, in the range of $1200\text{--}1300 \text{ cm}^{-1}$, belongs to the C–N and C–C stretching absorptions and N–H and C–O bending absorptions [13, 17, 28]. In the spectra of the inorganic-organic biohybrid films, bands at 1090 cm^{-1} corresponding to the Si–O–Si asymmetric vibration provide evidence of TEOS being bonded to the structure [29]. Peaks at 1345 cm^{-1} and 1190 cm^{-1} belonging to B–O stretching and B–OH vibration indicate that boron has been incorporated into the polymeric network. The weak bands at 880 cm^{-1} indicate the presence of Si–O–B bonds, and absorptions at 810 cm^{-1} and 637 cm^{-1} are related to symmetric B–O–Si and asymmetric B–O–B bond vibrations, respectively [30, 31]. The appearance of new bands relating to boron and silicon compounds in

the inorganic-organic hybrids shows that sol-gel reactions were successfully carried out.

Solid state ^{29}Si and ^{11}B NMR spectra of Si-B-WK/JFC hybrid films are given in figures 3(B) and (C). Three characteristic types of active centers, named geminal groups (Q_2 ; chemical shift $\delta = -91 \text{ ppm}$), free and bonded groups (Q_3 ; chemical shift $\delta = -101 \text{ ppm}$), and siloxane groups (Q_4 ; $\delta = -110 \text{ ppm}$), are identified in the ^{29}Si -CP-MAS NMR spectra of organic-inorganic hybrid molecules synthesized via sol-gel reactions [11, 12, 32]. The Q_4 characteristic peak belonging to siloxane bonds ($\text{Si}(\text{OX})_4$, $X = \text{Si}$, and B) was observed at approximately -110 ppm [33]. The chemical shift at -98.815 ppm refers to the Q_3 peak resulting from $\text{Si}(\text{OX})_3\text{OR}$ (functional groups such as $X = \text{Si}$, $R = -\text{OH}$, $-\text{NH}_2$, $-\text{SH}$) bonds [11]. This peak mainly exhibits the Si–O–R bonds formed due to reactions between rTEOS and functional groups in the WK/JFC.

^{11}B MAS NMR spectra contain trigonal (BO_3 groups, ^3B) and tetrahedral (BO_4 groups, ^4B) boron species. A narrow peak, usually at 0 ppm , represents tetrahedral boron species ($\text{B}(\text{OSi})_4$) surrounded by silicon atoms. However, when the boron atoms in the ^4B structure are replaced by silicon atoms, a chemical shift of $2\text{--}3 \text{ ppm}$ is observed. Therefore, a distinct peak seen in the spectrum around 3.757 ppm corresponds to ^4B -(2B, 2Si) or ^4B (1B, 3Si) species [12, 32, 34]. The other three distinct peaks seen in the spectrum belong to ^3B species. The different chemical shift values at 11.5 ppm , 15.6 ppm , and 17.29 ppm represent $\text{B}(\text{OSi})_3$, $\text{B}(\text{OSi})_2\text{OH}$, and $\text{BOSi}(\text{OH})_2$ structures, respectively. As can be seen in figure 3(C), as the number of B–O–Si bridges increases, the chemical shift values of trigonal boron decrease. It can also be seen that as the chemical shift values increase, the silicon content in the structure decreases [12, 34, 35].

XRD analysis was carried out to elucidate the materials' crystallinity degree; the results are shown in figure 3(D). The amorphous peak at about $2\theta = 20^\circ$ belongs to the β -sheets structures in WK and PS-JF extracts [36, 37]. However, the characteristic peak around $2\theta = 9^\circ$ related to α -helix structures was not observed in the XRD pattern of the WK extracts. This might be explained by damage to the protein backbone and these structures during extraction [37]. On the other hand, the broadband centered at $2\theta = 20\text{--}25^\circ$ in the inorganic-organic hybrid materials patterns represents the amorphous structure of silica. Additionally, the peaks at $2\theta = 43^\circ$ and 62° are characteristic peaks that prove the incorporation of the boron in the structure [38].

Thermal analyses of WK, PS-JFC, and sol-gel based inorganic-organic hybrid films have been studied, and the resulting thermograms are given in

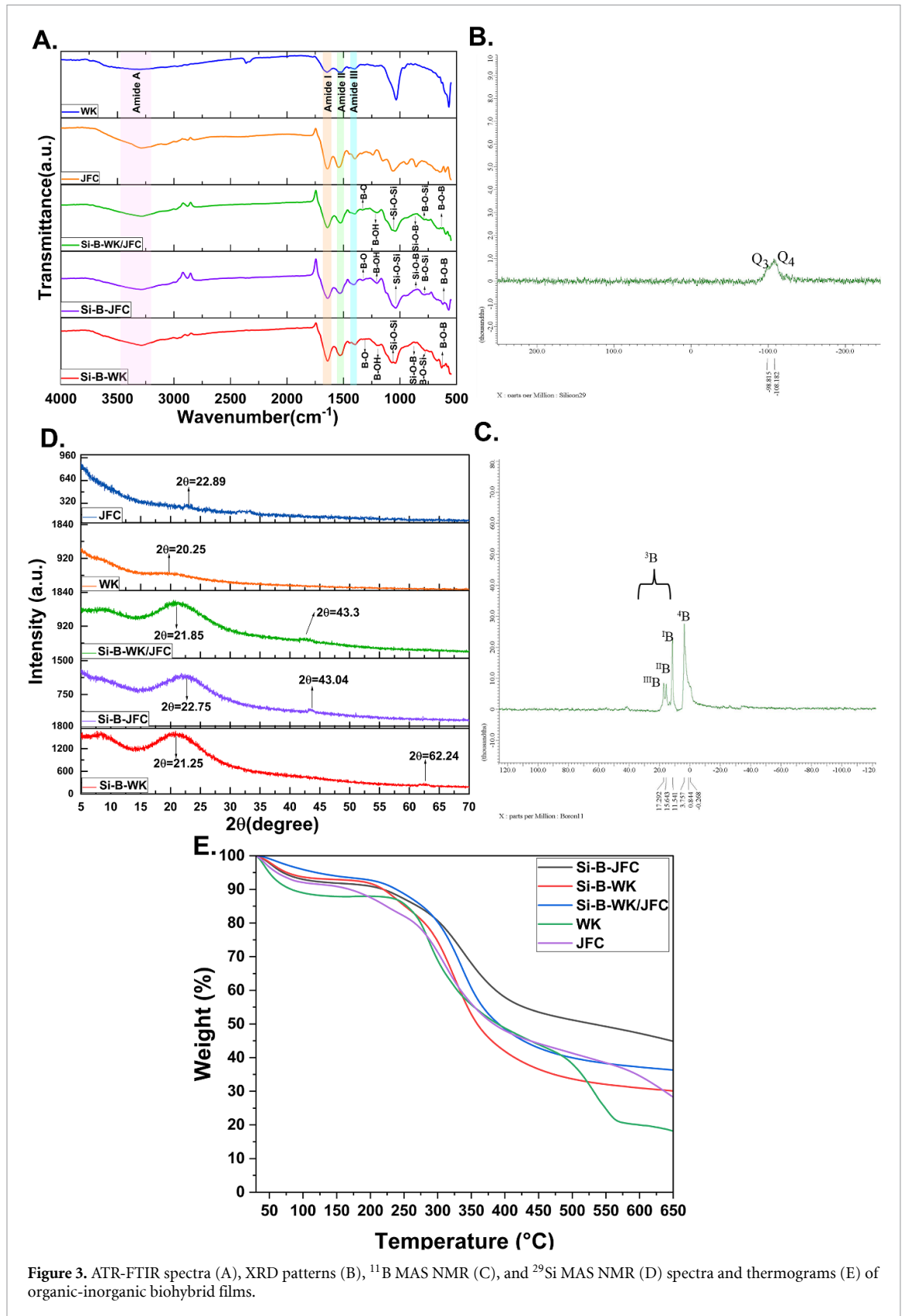
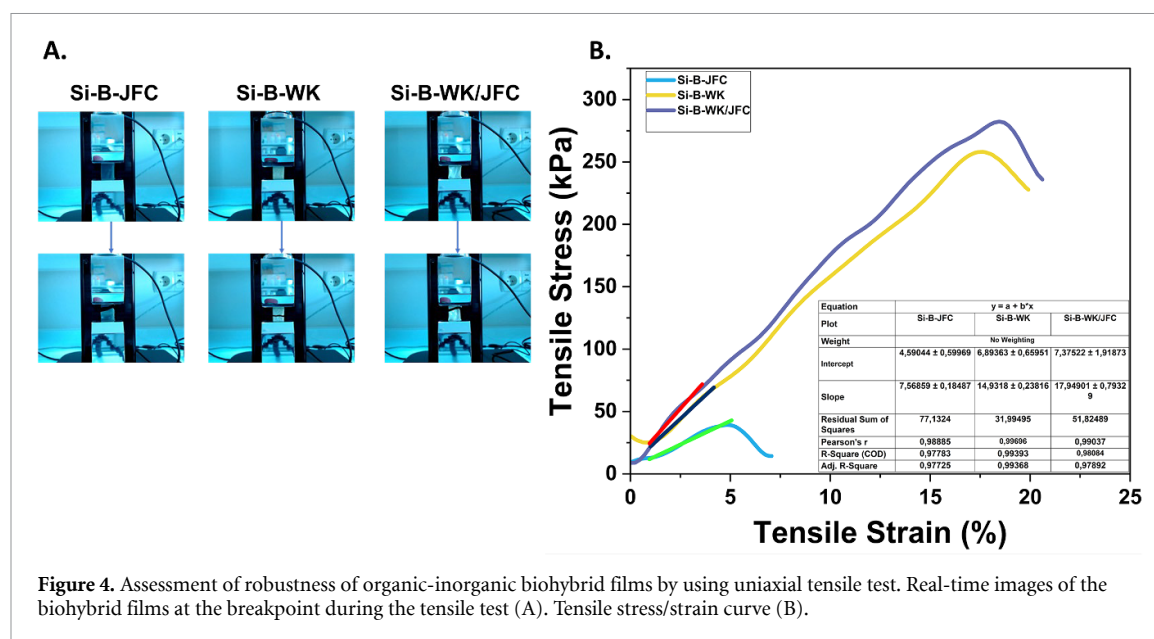


Figure 3. ATR-FTIR spectra (A), XRD patterns (B), ¹¹B MAS NMR (C), and ²⁹Si MAS NMR (D) spectra and thermograms (E) of organic-inorganic biohybrid films.

figure 3(E). The mass losses seen in the curves of all samples at temperatures below approximately 100 °C indicate the removal of structurally bonded water. The thermal degradation curves of WK and PS-JFC are relatively similar and appear

to lose about 80% and 60% of their mass weight, around 600 °C. Thermograms show that WK has a weaker structure than PS-JFC, as it undergoes more thermal degradation at the same temperature. This explains why the thermal stability of the Si-B-JFC



composite film decreases with the addition of WK [17]. Furthermore, mass losses at 600 °C for Si-B-WK, Si-B-JFC, and Si-B-WK/JFC are 50%, 30%, and 40%, respectively. Compared to WK and PS-JFC extracts, the increased thermal stability of the inorganic-organic hybrid films produced is evidence of successfully incorporating the boron and silicon into the polymeric network through sol-gel reactions.

Specific surface area and porosity parameters of hybrid films were investigated using the BET and BJH techniques. The data in table S2 clearly shows that the Si-B-WK/JFC film had a larger surface area than the Si-B-WK film. Thus, the results uncover a more comprehensive interconnected porous network was formed with the incorporation of PS-JFC into the hybrid films.

A higher surface area is generally associated with superior wettability. This characteristic, in turn, promotes the initial stages of cell adhesion, proliferation, and differentiation [39].

Moreover, we compared the mechanical properties of the single-component films with their composite counterparts. Wet films were used for these analyses as the film is too brittle to be subjected to the tensile deformation tests. Uniaxial tensile tests were performed until the point of breakages as shown in figure 4(A), and the force-displacement data were recorded for each hybrid film.

The tensile stress and Young's modulus of freestanding inorganic-organic hybrid films were measured. The results are shown in figure 4(B). As can be seen in the stress-strain curves, the ultimate tensile stress was 38.40, 257.99, and 282.36 kPa for the Si-B-WK/JFC, Si-B-WK, and Si-B-WK/JFC biohybrid films, respectively. The Si-B-WK/JFC biohybrid films

displayed a noticeable increment in Young's modulus compared to Si-B-WK and Si-B-JFC. Strain at break percentage was also determined to assess the deformation behavior of the hybrid films (table S1). Based on the stress-strain curve, Si-B-WK/JFC film was considered the most robust as it exhibited a maximum stress value of 282.36 kPa and a strain value of 18.45% at the breaking point. Zuniga *et al* made the collagen/keratin multi-protein hydrogels and reported that the critical factor influencing the enhancement in mechanical strength of the composite material is the collagen concentration rather than keratin concentration [40]. Glycerol is a prevalent plasticizer in producing proteinaceous films, employed in concentrations of 15%–50% parallel to protein mass. Its role is to enhance film flexibility by mitigating intramolecular and intermolecular attraction forces, thereby facilitating the mobility of polymeric chains [41]. However, some studies on the effect of adding glycerol on the mechanical properties of keratin and collagen-based films have reported that as the number of glycerol increases, the tensile strength decreases while the elongation at a break increase [42, 43]. In the work presented here, Si-B-WK/JFC film exhibited lower mechanical properties than Si-B-WK film. Combining the results mentioned above, two possible explanations arise for this phenomenon. The first explanation is that the protein amount in the Si-B-PS-JFC film is halved (5% w/v), and the second explanation is the use of excess glycerol despite the low protein amount. A previously published work established that the marine source collagen film with 2% (w/v) of glycerol and collagen had the 200 kPa maximum tensile stress [44]. In another study, wool-sourced keratin film was fabricated without adding glycerol,

and the maximum tensile stress was 486 kPa [45]. Considering the excess glycerol used in our study, the mechanical properties of our inorganic-organic hybrid Si-B-WK/JFC films containing collagen and keratin align with the findings from the mentioned studies. In addition, it can be said that incorporating -Si and -B elements in biohybrid films positively contributes to mechanical strength.

3.3. *In vitro* biodegradation study

Biomaterials with suitable degradation rates are good candidates for regenerative processes. Tracking of degradation rates provides essential clues to predict the behavior of materials *in vivo*. To this end, the biodegradability of the inorganic-organic biohybrid films was determined by following a protease treatment for 3 and 7 d of incubation. Obtained results are summarized as a percentage of weight loss in table S2. The total weight loss of B-Si-WK, Si-B-JFC, and Si-B-WK/JFC inorganic-organic hybrid films were found to be $15 \pm 1.15\%$, $57.21 \pm 6.57\%$ and $39.41 \pm 2.53\%$ on day 3, respectively. On the other hand, it was seen that the weight loss of the same hybrid films increased significantly after 7 d of incubation and the highest increase was in the collagen film, with a mass loss rate of $81.99 \pm 2.52\%$. Increasing structural features, such as porosity, hydrophilicity, and total surface area in the biomaterials, increase the water uptake capacity, rendering the biomaterial more susceptible to hydrolytic attacks [12, 46]. Considering the relationship between increasing total surface areas and biodegradation rates of hybrid films, we can conclude that the results are consistent.

3.4. SEM-EDS observations

SEM-EDS technique was used to evaluate the surface morphology and elemental composition of the inorganic-organic hybrid films. SEM micrographs at 250x and 50000x magnifications are given in figure 5(A). All hybrid films displayed a rough appearance and uniform distribution over the surface. In the EDS spectrum, the atomic mass percentages of the elements on all hybrid film surfaces are similar regarding carbon, oxygen, and nitrogen, which proves proteinaceous content. Additionally, both Si-B-WK and Si-B-WK/JFC inorganic-organic biohybrid films also exhibit composition of 0.5% sulfur, indicating keratin content in the structures. Furthermore, boron and silicon were detected in the EDS spectrum of all the hybrid films, proving that the organic-inorganic network within the hybrid films successfully occurred through sol-gel reactions. On the other hand, the elemental mapping for all

inorganic-organic hybrid films given in figure 5(B) shows the distribution of boron and silica atoms over the surface is homogeneous.

3.5. *In ovo* CAM assay

The CAM assay is a well-known *in vivo* system to study the effects on both pro- and anti-angiogenic response and biocompatibility of materials for regenerative strategies and tissue engineering applications. Furthermore, a straightforward observation of angiogenesis was performed by macroscopic, microscopic, and histological evaluation of all biohybrid films using the CAM assay *in vivo* animal model (figures 6(A)–(D)). Stereomicroscopic images revealed that transparent biohybrid films seen on the CAM surface in EDD7 maintained their structural integrity although swollen slightly in the aqueous environment after the 3 d of incubation (EDD10).

ImageJ software was used to calculate the density and index of newly formed vessels in a designated area around the biohybrid films. By using the binary images with a black-white scale, the blood vessel density index for the Si-B-WK, Si-B-JFC, and the Si-B-WK/JFC was calculated as 1.8 ± 0.092 , 3.02 ± 0.041 and 2.89 ± 0.054 , respectively. Based on the statistical analysis, there were no significant differences between the vascular index values of Si-B-WK/JFC and Si-B-JFC biohybrid films. However, the vascular index was increased significantly with the inclusion of collagen in the biohybrid structure. We reasoned that the Si-B-WK/JFC biohybrid films with a high surface-area-to-volume ratio provide more interconnections for cellular infiltration and vascular formation. Moreover, collagen, the primary component of the dermis, promotes growth and endothelial cell proliferation and migration [47]. This explains why a higher vascular index is observed in collagen-containing hybrid films.

SEM micrographs indicated that all biohybrid films supported blood cell adhesion, migration, and proliferation. On the other hand, microvascular networks were also observed on the surfaces of inorganic-organic biohybrid films containing collagen.

Hematoxylin and eosin staining were applied to investigate cellular structures in the CAM-biohybrid film tissue sections. The histological appearance revealed that the cell infiltration and development increased in the CAM-biohybrid film complex compared to the negative control groups. In addition, there was no evidence of acute or chronic inflammation, necrosis, or other unfavorable tissue in the biohybrid film-CAM complex, proving that the films were biocompatible [48].

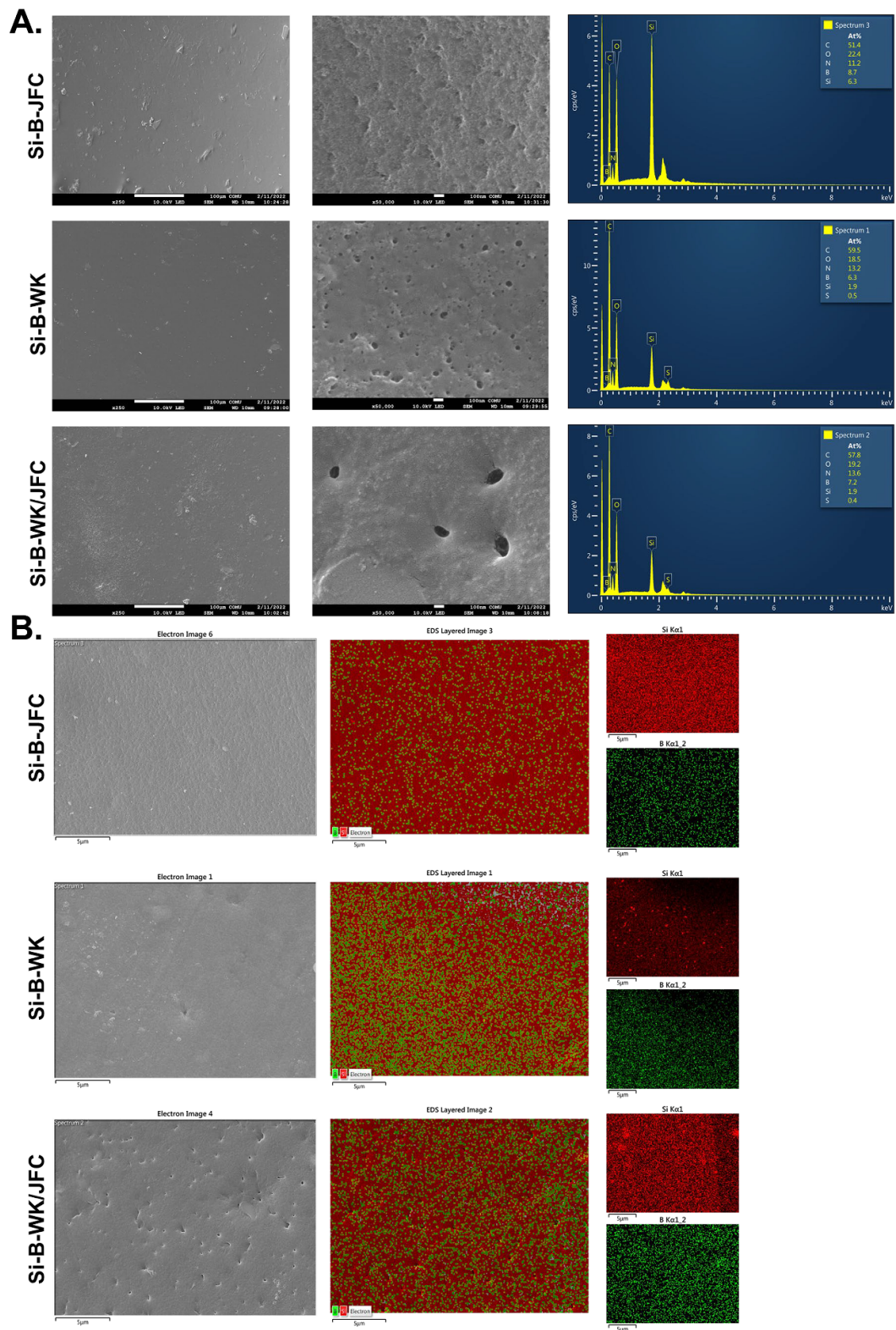
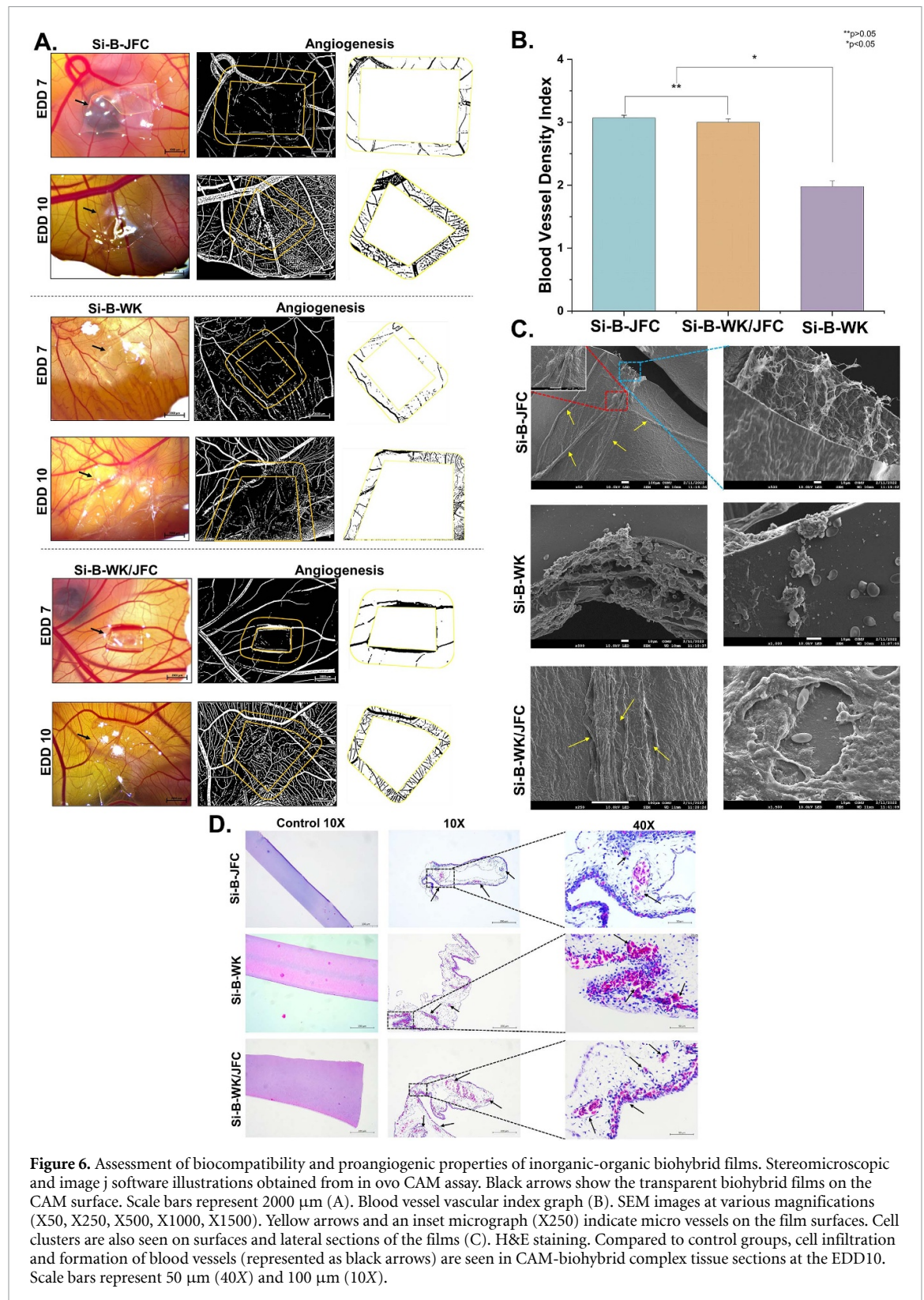


Figure 5. The SEM micrographs at X250, X50000 magnifications and EDS spectra (A), and elemental mappings (B) for silicon (red) and boron (green) of the organic-inorganic biohybrid films surfaces.



4. Conclusions

The work presented here demonstrates the synthesis of organic-inorganic hybrid films incorporating silicon and boron through a practical sol-gel method. Proteinaceous organic biopolymers served as macromolecular soft templates for pore formation due

to their containing reactive functional groups ($-\text{OH}$, $-\text{COOH}$, $-\text{NH}_2$). These reactions, utilizing rTEOS as a silica precursor, were based on forming cross-links between B-Si structures and mixtures of keratin/collagen proteins. Within this framework, the synthesis of inorganic-organic hybrid films containing Si-B-WK and Si-B-JFC was conducted to explore the

influence of keratin and collagen in composite films. An in-depth investigation of all synthesized films' structural and mechanical properties was performed. Structural characterization revealed successful synthesis of the inorganic-organic polymeric network. Comparing the results of tensile tests performed to determine mechanical properties with literature findings, it was observed that adding glycerol increased the films' elongation. However, it also led to a significant reduction in their tensile strength. Despite the considerably higher glycerol used in our study, the obtained tensile strength values align with the literature findings, suggesting a positive contribution to mechanical strength from the incorporated B-Si network in the structure. The network of blood vessels is an essential component of the tissue environment, delivering nutrients and oxygen to neighboring cells. In ovo CAM test was conducted to assess biocompatibility and pro-angiogenic properties. Histological and microscopic evaluations revealed increased cell adhesion, proliferation, and migration on all synthesized biohybrid structures, with no observed adverse effects. Based on the results above, we concluded that the Si-B-WK/JFC composite inorganic-organic hybrid films exhibited superior specifications thanks to the incorporation of collagen. Collectively, these characteristics demonstrate that the optimized composite inorganic-organic biohybrid Si-B-WK/JFC films could serve as a promising biomaterial for soft tissue engineering applications, particularly in wound healing. Nonetheless, further investigation is necessary for this specific application.

Data availability statement

The data cannot be made publicly available upon publication because no suitable repository exists for hosting data in this field of study. The data that support the findings of this study are available upon reasonable request from the authors.

Acknowledgments

The authors thank the Çanakkale Onsekiz Mart University Scientific Research Projects Coordination Unit (Project ID: FYL-2022-3983) for the financial support and acknowledge the Çanakkale Onsekiz Mart University Science and Technology Application and Research Center (ÇOBILTUM) providing facilities for analysis. We also thank Mr. Yücel Okatalı (MER-TER Medical, Eskişehir, Türkiye) for the HC staining and Ms. Tugce Kurt for her support in the design of the figures.

Author contributions

Safiye Nur Yildiz: methodology, formal analysis, data process. Tugba Sezgin Arslan: methodology, material design, formal analysis, data process, writing-original

draft preparation. Yavuz Emre Arslan: conceptualization, project administration, methodology, material design, supervision, writing-review, and editing.

Conflict of interest

In the study mentioned above, the proposed method regarding keratin extraction from wool is related to a patent application (TPE 2014/02104, Turkish Patent & Trademark Office), which is corresponded by Dr Yavuz Emre Arslan and Dr Tugba Sezgin Arslan.

Ethics statement

Ethics committee approval is not required for this studyAcadem'c.

ORCID iDs

Safiye Nur Yildiz  <https://orcid.org/0009-0008-4896-5553>

Tugba Sezgin Arslan  <https://orcid.org/0000-0003-2547-6120>

Yavuz Emre Arslan  <https://orcid.org/0000-0003-3445-1814>

References

- [1] Fernández-Hernán J P, Torres B, López A J and Rams J 2022 The role of the sol-gel synthesis process in the biomedical field and its use to enhance the performance of bioabsorbable magnesium implants *Gels* **8** 426
- [2] Nikolova M P and Chavali M S 2019 Recent advances in biomaterials for 3D scaffolds: a review *Bioact. Mater.* **4** 271–92
- [3] Biswal T 2019 Biopolymers for tissue engineering applications: a review *Mater. Today Proc.* **41** 397–402
- [4] Lan L, Ping J, Xiong J and Ying Y 2022 Sustainable natural bio-origin materials for future flexible devices *Adv. Sci.* **9** 2200560
- [5] Maia F R, Correlo V M, Oliveira J M and Reis R L 2019 Natural origin materials for bone tissue engineering: Properties, processing, and performance *Principles of Regenerative Medicine* 3rd edn (Academic Press) pp 535–58
- [6] Timorshina S, Popova E and Osmolovskiy A 2022 Sustainable applications of animal waste proteins *Polymers* **14** 1601
- [7] Arslan Y E and Kantarcioglu I 2019 Salvadoria persica extract-laden jellyfish collagen hybrid constructs for periodontal tissue regeneration *J. Turk. Chem. Soc. A* **6** 51–62
- [8] Pandey S and Mishra S B 2011 Sol-gel derived organic-inorganic hybrid materials: synthesis, characterizations and applications *J. Sol-Gel Sci. Technol.* **59** 73–94
- [9] Deshmukh K, Kovářík T, Křenek T, Docheva D, Stich T and Pola J 2020 Recent advances and future perspectives of sol-gel derived porous bioactive glasses: a review *RSC Adv.* **10** 33782–835
- [10] Owens G J, Singh R K, Foroutan F, Alqaysi M, Han C M and Mahapatra C, Kim H W and Knowles J C 2016 Sol-gel based materials for biomedical applications *Prog. Mater. Sci.* **77** 1–79
- [11] Yilmaz H D, Cengiz U, Arslan Y E, Kiran F and Ceylan A 2021 From a plant secretion to the promising bone grafts: cryogels of silicon-integrated quince seed mucilage by microwave-assisted sol-gel reaction *J. Biosci. Bioeng.* **131** 420–33

- [12] Cal F, Sezgin Arslan T, Derkus B, Kiran F, Cengiz U and Arslan Y E 2021 Synthesis of silica-based boron-incorporated collagen/human hair keratin hybrid cryogels with the potential bone formation capability *ACS Appl. Bio Mater.* **4** 7266–79
- [13] Kakkar P and Madhan B 2016 Fabrication of keratin-silica hydrogel for biomedical applications *Mater. Sci. Eng. C* **66** 178–84
- [14] Chupakhin O N et al 2017 Silicon–boroncontaining glycerohydrogel having wound healing, regenerative, and antimicrobial activity *Russ. Chem. Bull.* **66** 558–63
- [15] Perumal S, Ramadass S K and Madhan B 2014 Sol-gel processed mupirocin silica microspheres loaded collagen scaffold: a synergistic bio-composite for wound healing *Eur. J. Pharm. Sci.* **52** 26–33
- [16] Oh J S and Lee E J 2019 Engineered dressing of hybrid chitosan-silica for effective delivery of keratin growth factor and acceleration of wound healing *Mater. Sci. Eng. C* **103** 109815
- [17] Arslan Y E, Sezgin Arslan T, Derkus B, Emregul E and Emregul K C 2017 Fabrication of human hair keratin/jellyfish collagen/eggshell-derived hydroxyapatite osteoinductive biocomposite scaffolds for bone tissue engineering: from waste to regenerative medicine products *Colloids Surf. B* **154** 160–70
- [18] Derkus B, Arslan Y E, Bayrac A T, Kantarcioglu I, Emregul K C and Emregul E 2016 Development of a novel aptasensor using jellyfish collagen as matrix and thrombin detection in blood samples obtained from patients with various neurodisease *Sens. Actuators B* **228** 725–36
- [19] Yuan C J and No W J 2004 Application of TEOS/PDMS ormosil in the fabrication of amperometric biosensor *IEEE Int. Workshop on Biomedical Circuits and Systems (BIOCAS) Singapore 2004 S1/4/INV-S1/4/1*
- [20] Isik M et al 2023 3D printing of extracellular matrix-based multicomponent, all-natural, highly elastic, and functional materials toward vascular tissue engineering *Adv. Healthcare Mater.* **12** 2203044
- [21] Samancioglu A, Aydin B, Ozudogru E and Arslan Y E 2023 Evaluating the angiogenic and mechanical properties of hydrogels and physical constructs derived from spinal cord meninges extracellular matrix *Mater. Res. Express* **10** 085401
- [22] Sokolenko E A, Berchner-Pfannschmidt U, Ting S C, Schmid K W, Bechrakis N E, Seitz B, Tsimpaki T, Kraemer M M and Fiorentzis M 2022 Optimisation of the chicken chorioallantoic membrane assay in uveal melanoma research *Pharmaceutics* **14** 13
- [23] Ribatti D 2017 The chick embryo chorioallantoic membrane (CAM) assay *Reprod. Toxicol.* **70** 97–101
- [24] Tasaki K 2020 A novel thermal hydrolysis process for extraction of keratin from hog hair for commercial applications *Waste Manage.* **104** 33–41
- [25] Shavandi A, Silva T H, Bekhit A A and Bekhit A E D A 2017 Keratin: dissolution, extraction and biomedical application *Biomater. Sci.* **5** 1699–735
- [26] Zhou L T, Yang G, Yang X X, Cao Z J and Zhou M H 2014 Preparation of regenerated keratin sponge from waste feathers by a simple method and its potential use for oil adsorption *Environ. Sci. Pollut. Res.* **21** 5730–6
- [27] Silva R et al 2014 Hybrid hydrogels based on keratin and alginate for tissue engineering *J. Mater. Chem. B* **2** 5441–51
- [28] Tonin C, Zoccola M, Aluigi A, Varesano A, Montarsolo A, Vineis C and Zimbardi F 2006 Study on the conversion of wool keratin by steam explosion *Biomacromolecules* **7** 3499–504
- [29] Bramanti E, Bonaccorsi L, Campanella B, Ferrari C, Malara A and Freni A 2022 Structural characterization of electrospun tetraethylortosilicate (TEOS)/Polyvinylpyrrolidone (PVP) microfibrils *Mater. Chem. Phys.* **287** 126248
- [30] Siqueira R L, Yoshida I V P, Pardini L C and Schiavon M A 2007 Poly(borosiloxanes) as precursors for carbon fiber ceramic matrix composites *Mater. Res.* **10** 147–51
- [31] Islam E and Nebhani L 2021 Concerted effect of boron and porosity on shear thickening behavior of hybrid mesoporous silica dispersions *Mater. Today Chem.* **22** 100572
- [32] Angeli F, Charpentier T, De Ligny D and Cailleteau C 2010 Boron speciation in soda-lime borosilicate glasses containing zirconium *J. Am. Ceram. Soc.* **93** 2693–704
- [33] Ivanova Y, Vueva Y and Figueira M H 2006 Si-O-C-B amorphous materials from organic-inorganic hybrid precursors *J. Chem. Technol. Metall.* **41** 417–22
- [34] Du L S and Stebbins J F 2003 Nature of silicon-boron mixing in sodium borosilicate glasses: a high-resolution ¹¹B and ¹⁷O NMR study *J. Phys. Chem. B* **107** 10063–76
- [35] Fild C, Shantz D F, Lobo R F and Koller H 2000 Cation-induced transformation of boron-coordination in zeolites *Phys. Chem. Chem. Phys.* **2** 3091–8
- [36] Saska S, Teixeira L N, Tambasco De Oliveira P, Minarelli Gaspar A M, Lima Ribeiro S J, Messaddeq Y and Marchetto R 2012 Bacterial cellulose-collagen nanocomposite for bone tissue engineering *J. Mater. Chem.* **22** 22102–12
- [37] Wang J, Gao H, Qin C, Zhao Z, Yuan H, Wei J and Nie Y 2022 Experimental and theoretical study on the extraction of keratin from human hair using protic ionic liquids *J. Mol. Liq.* **368** 120626
- [38] Belaid H et al 2020 Boron nitride based nanobiocomposites: design by 3D printing for bone tissue engineering *ACS Appl. Bio Mater.* **3** 1865–74
- [39] Polini A and Yang F 2017 Physicochemical characterization of nanofiber composites *Nanofiber Composites for Biomedical Applications* (Elsevier Inc.) pp 97–115
- [40] Zuniga K, Gadde M, Scheffel J, Senecal K, Cressman E, Van Dyke M and Rylander M N 2021 Collagen/keratine multi-protein hydrogels as a thermally stable extracellular matrix for 3D *in vitro* models *Int. J. Hyperthermia* **38** 830–45
- [41] Langmaier F, Mokrejs P, Kolomaznik K and Mladek M 2008 Plasticizing collagen hydrolysate with glycerol and low-molecular weight poly(ethylene glycols) *Thermochim. Acta* **469** 52–58
- [42] Said M I, Erwanto Y and Abustam E 2016 Properties of edible film produced using combination of collagen extracts of bligon goatskin with glycerol *Am. J. Anim. Vet. Sci.* **11** 151–9
- [43] Moore G R, Martelli S M, Gandolfo C, Do Amaral Sobral P J and Laurindo J B 2006 Influence of the glycerol concentration on some physical properties of feather keratin films *Food Hydrocoll.* **20** 975–82
- [44] Abdullah J A A, Yemişken E, Guerrero A and Romero A 2023 Marine collagen-based antibacterial film reinforced with graphene and iron oxide nanoparticles *Int. J. Mol. Sci.* **24** 648
- [45] Mori H and Hara M 2018 Transparent biocompatible wool keratin film prepared by mechanical compression of porous keratin hydrogel *Mater. Sci. Eng. C* **91** 19–25
- [46] Qasim S B, Husain S, Huang Y, Pogorelov M, Deineka V, Lyndin M, Rawlinson A and Rehman I U 2017 *In-vitro* and *in-vivo* degradation studies of freeze gelled porous chitosan composite scaffolds for tissue engineering applications *Polym. Degrad. Stab.* **136** 31–38
- [47] Kim J H, Kim T H, Kang M S and Kim H W 2016 Angiogenic effects of collagen/mesoporous nanoparticle composite scaffold delivering VEGF165 *BioMed. Res. Int.* **2016** 1–8
- [48] Eke G, Mangir N, Hasirci N, MacNeil S and Hasirci V 2017 Development of a UV crosslinked biodegradable hydrogel containing adipose derived stem cells to promote vascularization for skin wounds and tissue engineering *Biomaterials* **129** 188–98